ADVANCED FUNCTIONAL MATERIALS
www.afm-journal.de

Precise Quantification of Angiogenesis in 3D Biomaterials Using in Vitro CAM Models: Enhancing 3Rs in Research and Minimizing in Vivo Dependency

*Ece Melis Er, Martha Patricia Pérez González, Beatriz Gil Garrido, Jasmine Ho, Hae-Won Kim, Jonathan Campbell Knowles, Jia Hua, Ferdinand Lali, and Prasad Sawadkar**

The efficacy of tissue engineering applications depends on selecting a scaffold with angiogenic properties, as angiogenesis plays a pivotal role in delivering nutrients and oxygen to cells for proper function. This study employed the chorioallantoic membrane (CAM) assay as a 3R-compliant model to investigate angiogenesis within an elastin-fibrin scaffold. Angiogenesis was evaluated in 2D using ImageJ software and in 3D using Micro-CT and confocal microscopy, respectively, following the intravascular injection of the contrast agents Indocyanine Green (ICG) and Microfil to quantify the vascular volume. Furthermore, we compared CAM analysis with in vivo vascularization using Optiray 350, an iodine-based contrast agent. Our findings highlight the limitations of 2D quantification and identify significant differences in vascular volume quantification between Microfil and ICG ($p < 0.05$). Specifically, ICG is distributed uniformly throughout the vascular network, unlike Microfil and Optiray 350, which have limited penetration in the microvessels within scaffolds. Our findings present a refined method for high-resolution, 3D visualization and quantification of vascular networks within biomaterials by CAM. This approach enables rapid assessment of angiogenic potential, thereby significantly reducing reliance on animal testing. By supporting the principles of the 3Rs, this strategy offers a more ethical and scalable framework for preclinical biomaterial evaluation.

1. Introduction

Angiogenesis is a critical process in tissue engineering, which involves the formation of new blood vessels from pre-existing ones. It plays a crucial role in developing and maintaining tissues and organs by providing oxygen and nutrients to cells and removing waste products. In tissue engineering, angiogenesis is a key factor in creating functional and viable engineered tissues.[1] Additionally, angiogenesis is a crucial stage in the progression of several life-threatening diseases, such as cancer and cardiovascular diseases.[2]

In the quest to develop an ideal scaffold for healthcare applications, a major challenge is to ensure an adequate blood supply to sustain the cells within the engineered material.[3] Without a proper vascular network, the innermost cells of the scaffold may be deprived of oxygen and nutrients, leading to cell death and, ultimately, the failure of the engineered tissue.

E. M. Er
Faculty of Dentistry
Oral and Craniofacial Sciences
King's College London
29 Weston St, London SE1 9SP, UK

E. M. Er, J. Ho, J. Hua, P. Sawadkar
Division of Surgery and Interventional Science
University College London
43-45 Foley St, London W1W 7TY, UK
E-mail: prasad.sawadkar@ucl.ac.uk

The ORCID identification number(s) for the author(s) of this article can be found under https://doi.org/10.1002/adfm.202503722

DOI: 10.1002/adfm.202503722

E. M. Er, M. P. P. González, B. G. Garrido, J. Hua, F. Lali, P. Sawadkar
The Griffin Institute
Northwick Park Institute for Medical Research
Northwick Park and St Mark's Hospitals
London HA1 3UJ, UK

H.-W. Kim, J. C. Knowles
Institute of Tissue Regeneration Engineering (ITREN)
Dankook University
Cheonan 330–714, Republic of Korea

J. C. Knowles, F. Lali
UCL Eastman Dental Institute
University College London
Rowland Hill Street, London NW3 2P, UK

M. P. P. González
Escuela de Ingeniería y Ciencias, Av. Eugenio Garza Sada 2501 Sur 64849
Tecnológico de Monterrey
Monterrey, Nuevo León 64849, Mexico

However, presently, there are no gold standards to assess these mechanisms. Considering this, accurate quantification of angiogenesis is imperative when evaluating different therapeutic modalities and improve our understanding of disease progression.

Implanted/engrafted scaffolds require the formation of new blood vessels to transport nutrients and oxygen to cells. For optimal perfusion, most body tissues require a highly branched blood vessel system, with optimal branch distances of less than 200 µm.[4] Yet, skin and cartilage are exceptions as they can acquire necessary oxygen and nutrients via diffusion from a more distant blood vessel, making them the only successful examples of clinical in vitro engineering.[5] Furthermore, poor angiogenesis is one of the main reasons why the clinical translation of tissue-engineered constructs is limited.[3,4]

To address this challenge, selecting an appropriate scaffold material is critical. Extracellular matrix (ECM)-derived biomaterials are often chosen for this purpose due to their ability to mimic native environment intrinsic physical and mechanical properties, high biocompatibility, and controlled degradation rate.[6] The angiogenic properties of different natural polymers such as collagen, fibrin, elastin, hyaluronic acid, and silk have already been assessed and reviewed elsewhere.[6,7] Out of all available ECM-derived biomaterials, fibrin is widely used as a transient matrix to promote vascularization during tissue engineering.[8] During the first stages of wound healing, fibrin-precursor fibrinogen is recruited and activated to form a fibrin-rich clot in the wound site. The fibrin matrix has a high affinity for growth factors, namely vascular endothelial growth factor (VEGF) and cell surface proteins like integrins, promoting cell adhesion, endothelial growth, and overall tissue regeneration.[8,9] In tissue engineering, these properties have been exploited to enhance graft angiogenesis and integration for different purposes.[10] In addition, scaffold porosity has also been shown to influence vascularization rate.[11] It has been suggested that larger pores allow for improved cellular infiltration and endothelial cell adhesion to form vessel-like structures.[12] Therefore, composition and 3D architecture of scaffolds are key to ensure full integration and functionality of grafts after implantation.

Various methods are currently employed to evaluate neovasculature, with in vitro assays often preferred due to their practicality, cost-effectiveness, and ability to generate quantitative data. Common examples include the tube formation assay, which assesses the ability of endothelial cells to form capillary-like structures, and the Matrix Metalloproteinase (MMP) assay, which evaluates the role of ECM remodeling in angiogenesis.[13] While these in vitro models are valuable for preliminary studies, they fail to replicate the complex biological interactions in living tissues, rendering their results less representative of true physiological processes.[13]

To overcome these limitations, there has been a shift toward in vivo models, which allow for the study of angiogenesis within the context of a living organism, providing a more accurate reflection of biological dynamics. Nonetheless, traditional in vivo assays, such as the corneal angiogenesis assay or the Matrigel plug assay, present challenges, including high costs, longer experimental timelines, and ethical considerations associated with animal use.[14] Scaffolds developed for tissue engineering applications undergo in vivo testing for their efficacy prior to clinical applications. According to the Royal Society for the Prevention of Cruelty to Animals (RSPCA) data for 2021, every year, more than 100 million animals worldwide are used for experimentation, and~3 million are used in the UK. During these experiments, animals experienced pain, suffering, and distress. The severity of these experiences was reported as 22% moderate and 3% severe. To minimize the number of animals and their suffering during experimentation, a model compliant with the 3Rs (replacement, reduction, and refinement) principles should be promoted/adopted in the research. Additionally, a 3D evaluation, instead of 2D, must be assessed considering the varied depth of infiltration of blood vessels within the scaffolds that closely resemble the physiological vessel infiltration when implanted into humans.

To address this, the use of the chorioallantoic membrane of chicken embryos (CAM assay) is currently favored as an in vivo model that, due to the lack of a fully developed neural system in the chicken embryo's early developmental stage, it is considered a borderline between in vitro and in vivo systems and not regulated under ASPA (Aminals Scientific Procedures Act1986). Therefore, it complies with the 3R principles.[15] Although the current method of choice to quantify angiogenesis in the CAM model is based on 2D image analysis software,[2a] CAM angiogenesis could be captured with advanced imaging modalities like micro-computed tomography (Micro-CT), which enables better visualization and evaluation of angiogenic processes in 3D.[16]

To achieve this, a radio-opaque medium would be required for the perfusion of the vessels as a contrast agent, but this procedure entails technical challenges. For instance, it may not ensure complete and uniform filling of all the vessels, leading to incomplete visualization of the vascular network. Moreover, the incomplete injection of the contrast agent may result in quantitative inaccuracies that may cause inconsistencies in data obtained by Micro-CT.[17] In a previous study by Woloszyk et al., the perfusion efficacy of Microfil, a commonly used radio-opaque medium, was addressed. As the first perfusion was incomplete, a second perfusion of the dye was needed to visualize the complete vascular system.[16] In another study conducted by Kurz et al., 3D images obtained by dual immunostaining allowed observation of arteries and veins; however, the microvessels were not detected. Therefore, the staining was incomplete.[18]

These limitations suggest that a novel staining agent and technique are required to improve the accuracy of the evaluation of angiogenesis in biomaterials. Indocyanine Green (ICG) dye is a fluorescent dye that exhibits a strong affinity for plasma proteins, leading to its sequestration within the vascular system.[19] This

H.-W. Kim
Department of Nanobiomedical Science and BK21 NBM Global Research Center for Regenerative Medicine
Dankook University
Cheonan 31116, Republic of Korea
H.-W. Kim
Mechanobiology Dental Medicine Research Center
Dankook University
Cheonan 31116, Republic of Korea
H.-W. Kim, J. C. Knowles, P. Sawadkar
UCL Eastman-Korea Dental Medicine Innovation Center
Dankook University
Cheonan 31116, Republic of Korea

unique property of ICG dye makes it an excellent candidate for the development of an alternative 3D angiogenesis assay.

This research aimed to compare the comprehensive 3D data obtained with two advanced imaging techniques (Micro-CT and confocal microscopy) versus 2D data acquired from scaffold image analysis on the CAM surface and to compare the 3D data of Micro-CT using Microfil dye with the 3D data of confocal microscopy using ICG dye, ultimately determining which method is more accurate for quantifying 3D angiogenesis.

To assess the effectivity in angiogenic evaluation following the developed protocols, it was important to fabricate a pro-angiogenic scaffold model to ensure proper vascularization of the samples. In this study, we initially employed a fibrin-only scaffold due to fibrin's widely established role in promoting angiogenesis. Previous work also demonstrated the high angiogenic capacity of this model.[20] However, preliminary tests revealed that fibrin scaffolds exhibited poor mechanical stability and rapid degradation when placed on the surface of the CAM, limiting their suitability for implantation and imaging.

Instead, the study was followed with elastin–fibrin (EF) scaffolds due to its biomimetic properties, which closely resemble the native ECM, providing structural support and biochemical signals essential for promoting angiogenesis. EF scaffolds had previously been demonstrated to exhibit a significant level of vascularization in vivo, highlighting their strong pro-angiogenic properties and making them an ideal choice for evaluating angiogenic responses in the CAM model.[21]

2. Results

2.1. Material Characterization of Scaffold

During the initial phase of this study, scaffolds were fabricated using fibrinogen alone, without any cross-linking agent. Fibrin was selected due to its well-established role in promoting angiogenesis, making it a relevant biomaterial for vascularization studies. Scaffolds (10 mm diameter) were cast and freeze-dried to achieve a porous structure. However, following lyophilization, the fibrin-only scaffolds displayed irregular morphology and significant structural collapse, losing their spherical surface and uniform shape (**Figure** 1A,B). Upon implantation on the CAM, these scaffolds further degraded and became difficult to locate, appearing flattened and indistinct. Post-dissection measurements revealed that their diameter had decreased by ~ 50%, from 10 to 5 mm. Given their decreased stability and a thickness by 0.5 cm, these scaffolds were deemed unsuitable for the reliable assessment of 3D angiogenesis. To address these limitations, a modified scaffold composition was developed by blending fibrin with elastin and cross-linking the mixture using glutaraldehyde, resulting in fibrin–elastin (EF) scaffolds with improved structural integrity. These EF scaffolds were used for all subsequent experimental analyses. To evaluate their physical properties, swelling ratio tests were conducted, quantifying the scaffold's capacity to absorb and retain solvent. Scaffolds were prepared by blending elastin with fibrin and cross-linking the mixture using glutaraldehyde to achieve the desired 3D matrix. We conducted swelling ratio tests to evaluate the interaction between the scaffold and solvent. The swelling ratio, defined as the ratio of the weight of the swollen polymer to its dry weight, quantifies the polymer's capacity to absorb and retain solvent. This metric provides insights into the scaffold's cross-linking density, porosity, and overall hydrophilicity. Upon submersion in water, the scaffolds exhibited pronounced morphological changes between the dry and wet fibrin states (Figure 1A,B). To elucidate these modifications, we employed scanning electron microscopy (SEM) for detailed surface topology analysis (Figure 1C,D). The analysis revealed notable differences in the pore characteristics of fibrin and EF scaffolds. Fibrin scaffolds exhibited a porosity of 44.23 ± 2.21%, while EF scaffolds demonstrated an increased porosity of 54.77 ± 10.13% (Figure 1E). Over 90% of pores across these scaffolds presented a thickness (diameter) that ranged from 17.93 to 89.65 µm, (Figure 1F)). Interestingly, EF scaffolds presented a smaller pore range, with ≈55% of pores separated by between 17.93 and 35.86 µm (Figure 1G). On the other hand, 40% of pores in the fibrin scaffold had a separation in the range of 35.86–89.65 µm, with over 20% within the pore range of 89.65–167.37 µm. Notably, the cross-linked EF scaffolds maintained their original 3D structure when applied to the CAM model (Figure 1H,I). The swelling ratio was determined to be 55.36% ± 1.22% for fibrin and 13% ± 1.48% for EF scaffolds, indicating a higher water absorption capacity for fibrin than EF (Figure 1J). Furthermore, after observing that the placement of cross-linked EF scaffolds on the CAM surface led to a reduction in embryo survival rates from 90% to 40%, we attributed this decrease to the potential toxicity of residual glutaraldehyde. To address this, we extended the washing duration by one hour, which effectively restored the survival rate to ≈87% in subsequent trials.

2.2. 2D Angiogenesis Analysis

The CAM assay was employed to evaluate the angiogenic response elicited by EF scaffolds. Following implantation (ED 10), the scaffolds ($n = 5$) were explanted on ED13 for vascular analysis (**Figure** 2A). Macroscopic examination revealed blood vessel infiltration, beginning with a prominent vessel at the scaffold's perimeter and extending toward its center (Figure 2B). Notable morphological differences were observed in the vascular patterns across the scaffolds; some exhibited a well-defined capillary plexus, while others showed minimal vascularization across the majority of the surface. Binary image analysis was conducted using ImageJ software to quantitatively assess the angiogenic potential of the EF scaffolds. Two primary metrics were measured: vessel area (mm^2) and vessel area fraction (%). Among all scaffolds, the maximum vessel area fraction observed was 5.864%, and the minimum was 3.94%. The mean vessel area was calculated to be ≈120.19 mm^2, with an average area fraction of 4.94%. Despite the evident heterogeneity in vascularization as reflected in the binary images, statistical analysis did not reveal significant differences in these parameters across different samples. It is important to note that these results reflect the vascularization present only on the surface of the scaffolds and do not confirm the extent of vessel penetration within the scaffold interior. Histological assessment of the scaffolds with H&E staining confirmed the presence of vessels within the scaffold matrix (Figure 2C). Histological analysis revealed that the majority of blood vessels infiltrating the EF scaffolds appeared to be

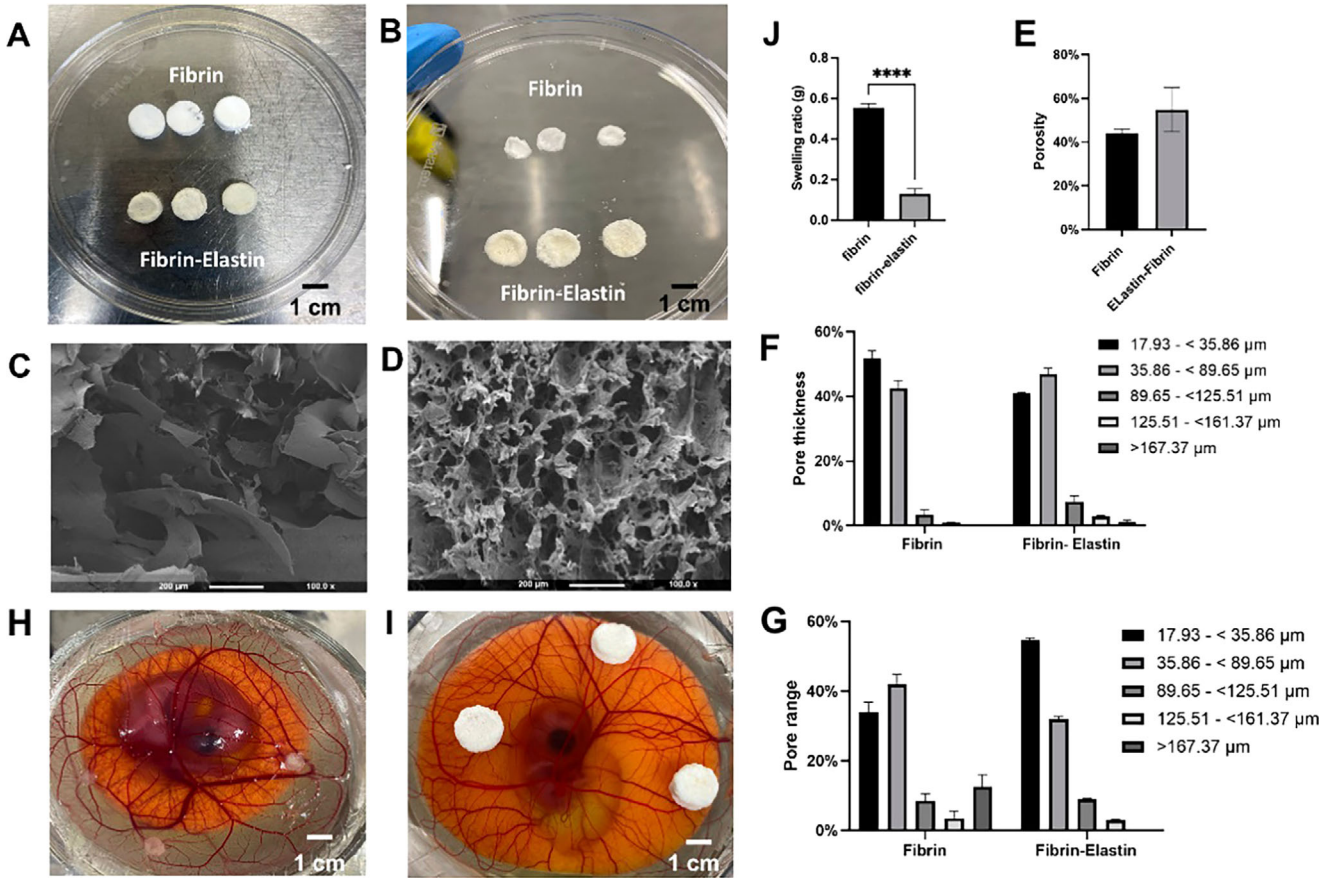

Figure 1. Preliminary characterization and comparison of fibrin-only and fibrin–elastin (EF) scaffolds to justify scaffold selection for downstream experimentation. The scaffolds in a desiccated state (A), the scaffolds post hydration (B). SEM images of fibrin (C) and EF (D) scaffolds. Graphical material characterization data showing swelling ratio (J), porosity (E), pore thickness (average pore diameter) measured across the scaffolds (F), and pore range (distribution of pore sizes) to reflect the range and frequency of individual pore diameters (G) for fibrin and EF scaffolds ($n = 3$). Implantation on the CAM surface, fibrin (H) and EF (I). It is imperative to acknowledge the discernible morphological distinctions observed between the two scaffold types upon placement on the CAM surface. A statistically significant difference is indicated by $p < 0.0001$(****). Scale bar at the bottom of the images.

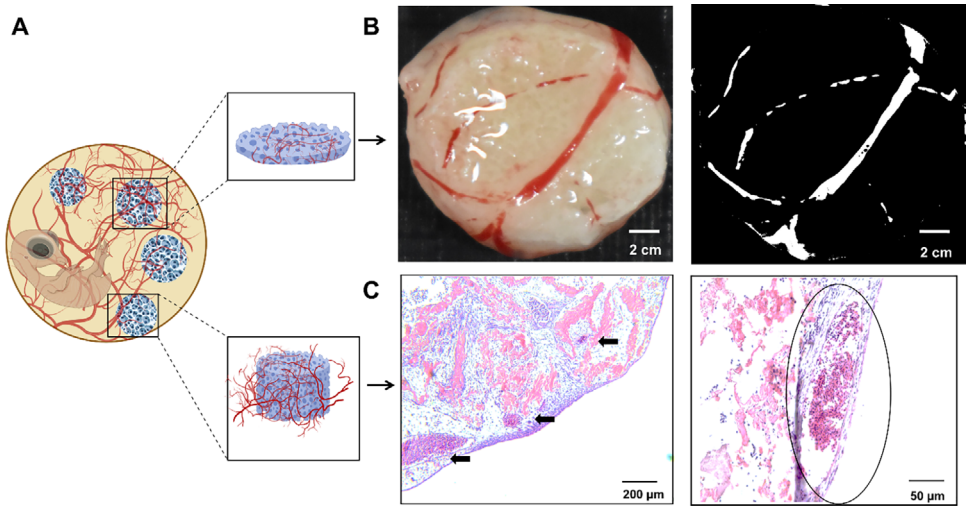

Figure 2. Schematic representative of CAM with scaffolds on (A), a macroscopic image of EF scaffold and its binary image (B, $n = 5$), and representative image of a H&E cross-section (C, $n = 3$). Blood vessels in image B are seen in red color on the left and on the right (white color over the black of the scaffold. In Figure 3C, black arrows indicate the vessels that are observed in histological cross sections but are not detected in the binary images (3B).

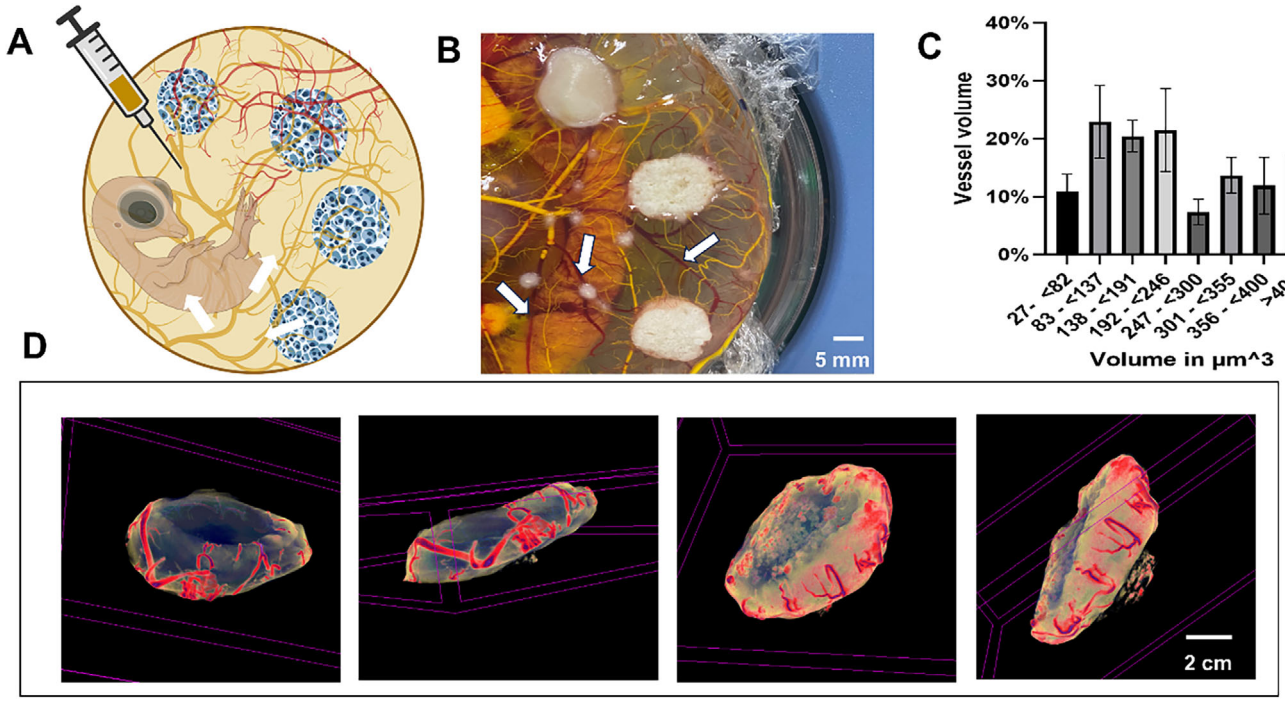

Figure 3. Schematic representation of CAM with scaffolds on ED13 and injecting microfil dye (A). Figure 4B shows amacroscopic image of the scaffold on CAM (ED14) following the perfusion. Perfused regions are yellow, and vessels are red, the white arrows point out the vessels which MicroFil did not reach Data are presented as mean values from three independent biological repeats ($n = 3$). Figure 4C presents the vascular thickness (vessel volume, measured in μm^3) distribution in the scaffold after CAM assay, measured with CTAn software after MicroCT scanner ($n = 3$). Figure 4D shows the representative 3D reconstruction of a scaffold obtained with Micro-CT scanner. Images were taken at the top and side view of the red color present inside the scaffold indicates the presence of vessels inside the scaffolds.

capillaries or small caliber vessels, based on their thin endothelial lining and small luminal diameter. No large arterioles or venous structures were evident within the scaffold pores at this early time point. A quantitative assessment of five histological sections revealed that the average vessel area occupied ≈4% of the scaffold volume. These results indicate that the 3D porous EF scaffolds effectively promote angiogenesis, facilitating successful vascular infiltration throughout the scaffold structure.

2.3. 3D Micro-CT Angiogenesis Analysis

We employed micro-CT as an imaging modality to investigate the vascularization of a 3D porous scaffold within the highly vascularized environment of CAM (**Figure** 3A). Furthermore, with this imaging technique, we conducted a comprehensive 3D analysis of the acquired data, and this was confirmed with micro-CT scans of three samples. The images obtained from scans showed that MicroFil perfused 3D vessels surrounding the sides of the scaffolds (Figure 3B), some showed the vascular elements incorporated inside the scaffold (Figure 3D) within 4 days of the ex ovo culture period. Using micro-CT imaging, we were able to visualize the entire vascular network surrounding the scaffold. In contrast, the macroscopic image of the same samples in ex ovo (Figure 2B) only reveals the surface vascularization observed on the CAM. Quantitative 3D analysis using CTAn software revealed distinct patterns of vascular thickness across all three scaffolds. Vessels measuring 83–246 µm in diameter were most prevalent, while those between 247 and 300 µm were comparatively rare. (Figure 3C).

2.4. 3D Confocal Microscopy Analysis

To quantify the angiogenesis induced by scaffolds in a 3D context, we employed a second method. This involved staining the scaffolds with ICG dye and visualizing them through in vivo fluorescent microscopy (**Figure** 4A). The data obtained from this method was also statistically analyzed using 3D data, vessel volume. Following the perfusion of 0.45 ml of ICG dye into the CAM, the immediate detection of dye perfusion was confirmed by the dark purple coloration of the CAM vessels. Dissected scaffolds were kept frozen and away from any light source until confocal microscopy was performed. The 3D confocal imaging produced a series of images where the scaffold was distinctly visualized in green, while the surrounding vessels appeared as darker structures, allowing for clear delineation between the scaffold and the vascular network (Figure 4B). This clear contrast allowed us to accurately identify the borders of the vessels at different depths during the optical sectioning process. Moreover, the presented images in Figure 4D represent the cross-sectional view of the scaffolds, specifically showing the vascular architecture both on the surface and within the scaffold matrix. By conducting a comprehensive analysis of these images, we successfully captured the entirety of the vascular network existing within the visualized area of the scaffolds. We found that we could capture micro to

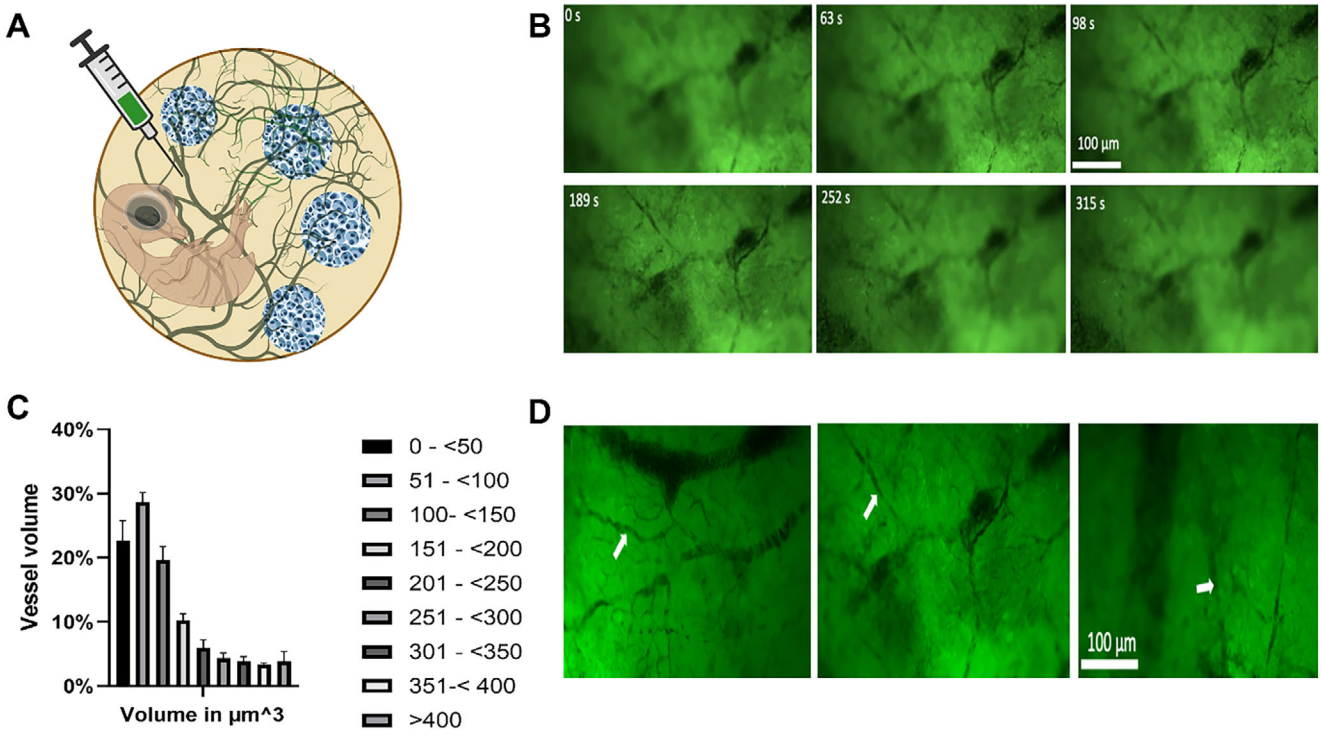

Figure 4. Schematic representative of CAM with scaffolds on ED13 and injecting ICG dye (A). Image displaying time-lapse images from the stack. The scaffold is highlighted in green, while the vessels appear dark, creating a noticeable contrast (B). A quantification of vessel volume (C). Representative confocal fluorescent images of scaffolds 60 min after the injection. Some of the vessels in the depth are indicated with white arrows (D). All experiments were conducted with a sample size of $n = 3$, representing three independent biological repeats.

macro-size vessels. A majority of vessels were present in the 1–150 µm (Figure 4C). Consequently, this assessment enabled us to accurately evaluate the extent of angiogenesis induced by the scaffolds, encompassing larger vessels and micro-vessels. However, it is important to note that due to the inherent imaging depth limitations of confocal microscopy, most vascular features analyzed in this study were concentrated on the surface and shallow regions of the scaffold. We employed macro programming in ImageJ software to achieve efficient volume measurements and repeated measurements across a complete stack (Supporting Information). The obtained results were compared with our previous findings from Micro-CT.

2.5. In Vivo Analysis

The post-mortem conducted on day 14 revealed that the implanted scaffold was successfully integrated into the host system, with blood arteries from the surrounding area vascularized the EF scaffold (**Figure 5**B), and gross analysis confirmed that blood vessels were infiltrated into scaffolds (Figure 5C). Angiography data under micro CT showed that Optiray 350 was able to penetrate into major vessels; however, we could not detect capillaries or microvessels (Figure 5D,E), indicating limited penetration of Optiray 350 and vessel volume between in the range of 0–500 µm was 3.9 ± 0.05%, and the maximum of vessels volume was detected 32.62 ± 2.51% in the range of 1001–1500 µm. However, in the range 501–1000 and 1501–2000 µm, it was 19.73 ± 2.81% and 26.75 ± 1.52%, respectively, and 18.69 ± 0.44% vascular volume was calculated >2000 µm (Figure 5F). These results showed vascularization detection primarily in larger vessels, with limited visualization of smaller microvasculature in 0–500 µm range due to the Optiray 350's limited permeability into finer vascular networks.

3. Discussion

In this study, we developed novel scaffolds using two of the natural polymers derived from the ECM: fibrin and elastin. It is crucial for tissue engineering applications to ensure that these scaffolds do not exhibit toxic effects on their surroundings as they degrade and are replaced by the host ECM niche after implantation.[22] Therefore, incorporating natural ECM proteins in the scaffolds offers advantages.[23] Among the three main components of the ECM, fibrin polymer was extensively studied and found previously to have excellent angiogenic properties; therefore, it was used as the main natural polymer of the scaffolds used for quantifying angiogenesis.[20] However, the preliminary results we obtained suggested that fibrin was not stable enough to fabricate 3D scaffolds which wouldn't collapse upon implantation on CAM. This outcome can be attributed to the polymer's swelling ratio, which measures its absorption capacity when immersed in a solvent. Our investigation revealed that fibrin exhibited significant absorbance (Figure 1), a conclusion that aligns with a separate study conducted in 2021.[20]

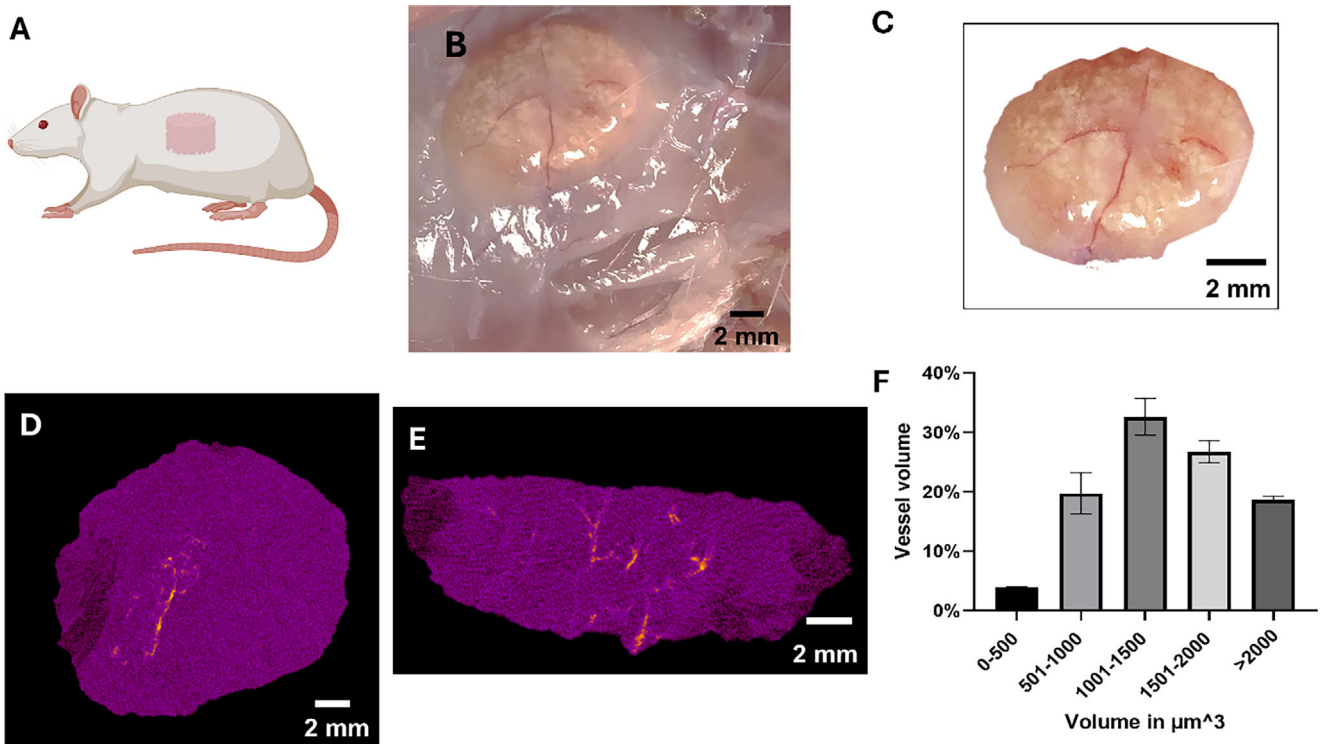

Figure 5. Showing in vivo implantation of EF scaffold (A), in vivo engraftment of scaffold and angiogenesis at 14 days (B), gross observation at 14 days (C), Micro-CT 3D analysis of the angiogenesis sagittal plane (D) and coronal plane (E), quantification of 3D angiogenesis % (F).

The previous study provided scientific justification for combining fibrin and elastin to create a composite scaffold that overcomes the individual limitations of both scaffolds, addressing the issue of instability in our 3D porous scaffolds. The researchers extensively examined the physicochemical characteristics of elastin, collagen, and fibrin. Their analysis, including calculations of swelling ratio and dynamic water contact angle, revealed that elastin scaffolds exhibited the lowest capacity for absorbing solvents.[20,21] This finding was consistent with the natural insolubility and hydrophobic nature of elastin.[24] However, it is important to note that the hydrophobic nature of the elastin scaffolds led to accelerated degradation in vivo, which consequently resulted in poor vascularization. In contrast, a subsequent study by the same group demonstrated that combining elastin with fibrin to form a composite scaffold significantly enhanced vascularization. The EF scaffolds exhibited a markedly higher level of vascular infiltration compared to single-component scaffolds, suggesting that the composite scaffold possesses strong angiogenic properties, likely due to the synergistic effects of both materials.[21]

Furthermore, we crosslinked the EF scaffolds with the most used crosslinking agent, glutaraldehyde (GA). Incorporating crosslinking into the composite material improved the stability of the FE matrix. Previous studies have demonstrated the effectiveness of GA in stabilizing scaffolds and enhancing the durability of ECM derived scaffolds.[25] Crosslinking with GA improved the EF matrix and gave a significantly (of $p < 0.0001$) lower swelling ratio compared to fibrin gel scaffolds (Figure 1J). However, the toxicity of GA caused complications during the first phase of our study.[25c] Upon implantation, EF scaffolds killed all the embryos, but this was later resolved by optimizing the washing protocol. Consequently, by incorporating both fibrin, elastin, and a crosslinking agent, we successfully developed 3D scaffolds that were stable and possessed highly angiogenic properties, which are advantageous for our specific objectives and study.

In this research, we selected the CAM assay due to its distinct advantages over traditional in vitro angiogenesis evaluation methods. While in vitro assays, such as the tube formation assay, MMP assay, and Matrigel Plug assay, are widely used, each has inherent limitations that constrain their ability to replicate in vivo angiogenesis accurately.[26] The tube formation assay, for instance, allows for the rapid assessment of endothelial cell behavior on a 2D matrix. However, it lacks the complexity needed to mimic the 3D environment and dynamic cellular interactions of living tissues, making it less representative of in vivo vascularization processes. Similarly, the MMP assay, though offering high-throughput analysis, is susceptible to inconsistent results due to variations in tube-forming capability across different endothelial cell groups. The Matrigel Plug assay provides quantifiable results and is technically straightforward but is time-consuming and prone to systematic errors during data analysis.

There are also alternative methods for angiogenesis analysis in vivo. The Von Willebrand factor (vWF) is a protein that is widely used as an angiogenic marker for immunofluorescence analysis. vWF plays a key role in blood vessel formation, promoting platelet adhesion and inhibiting clotting factor degradation during hemostasis.[27] Published work has already proven an increased VWF expression in response to activated endothelium.[28] Immunostaining of vMF is a well-accepted method for quantification of blood vessel infiltration

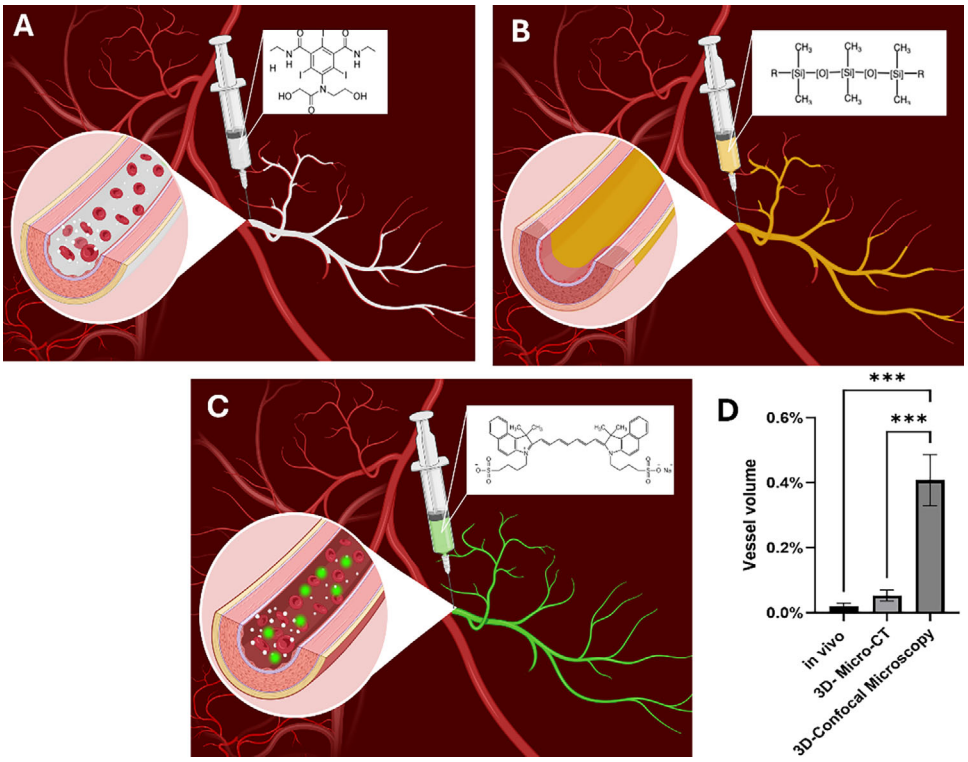

Figure 6. Shows the difference in vascular volume detected by three 3D imaging methods, in vivo Optiray 350 (A), Microfil (B), and ICG dye (C) with their 3D vessel volume quantification ($n = 3$), *** indicates the statistical significance of $p < 0.001$.

in tissue engineering.[12] Nevertheless, this method has several drawbacks. Although there is a correlation between blood vessel formation and vMF levels, the role of vMF in vascular health is not yet fully discerned;[27,29] hence the link between vMF and angiogenesis might not be as direct as initially thought. In addition, vMF analysis does not allow 3D analysis of vessel infiltration, limiting the results cross-sectional analysis.

By contrast, the CAM assay offers a physiologically relevant, 3D environment that supports the development of functional blood vessels with direct blood flow, closely mirroring in vivo conditions. This model enables a more realistic evaluation of vascular infiltration, maturation, and integration with the host vasculature, which traditional in vitro assays cannot achieve. The CAM model is also cost-effective, suitable for high-throughput screening, and minimizes the need for conventional animal models, hence complying with the principles of the 3Rs.[26] Its relatively short experimental timeline and ease of use make it ideal for investigating the angiogenic properties of biomaterials in a reproducible and ethically responsible manner, particularly during the initial phases of scaffold development.

The quantification of angiogenesis induced by scaffolds using the CAM model typically relies on 2D image analysis, considered the current gold standard.[30] In our study, the EF matrix was implanted on ED10, a developmental stage at which the embryo can tolerate implants.[31] The matrix remained on the CAM until ED14, allowing sufficient time for vascular infiltration. Subsequently, the samples were fixed and dissected, and to enhance contrast, they were placed on a black background. Consistency in image acquisition was ensured by capturing all images from the same distance using the same digital camera. Additionally, a ruler was employed for scale calibration. To improve vessel visibility, the images were split into channels. Among the various channels tested, the green channel was selected due to its higher contrast and signal strength, consistent with other studies.[32] Following the same methodology, we obtained similar results. The green channel image was further subjected to a bandpass filter, leveraging Gaussian filtering in Fourier space to enhance structural sharpness. This approach effectively isolated regions of interest (ROIs) by eliminating undesired ROIs of specified sizes, resulting in refined images suitable for analysis. In our study, the percentage of vascular area of the EF scaffolds was measured to determine the extent of blood vessel coverage on the scaffold's surface. This parameter directly correlates with the expansion of the vascular network. However, it is essential to consider the influence that vessel thickness has on the extent of this increase. During angiogenesis, newly formed vascular sprouts often exhibit a thin morphology, which may contribute minimally to the total vascular area.[33] One of the aims of our study was to demonstrate the superiority of 3D angiogenesis analysis over conventional 2D analysis in mimicking in vivo conditions. To address this aim, we compared the outcomes obtained from four different visualization techniques. All four techniques employed EF scaffolds with identical composition and structure, ensuring a similar angiogenic response. Notably, the data presented in **Figure 6D** exhibited significant variations among the techniques, particularly with the 2D analysis yielding the highest values. It is important to note that direct comparison between 2D and 3D results is not feasible since 2D results are expressed in area

fraction, while 3D results are expressed in volume fraction. Nonetheless, we can conclude that the 2D analysis is inaccurate because the vessels formed through in vivo angiogenesis possess volume and are not flat. Hence, for accurate quantification of angiogenesis induced by our scaffolds, it is imperative to consider vessel thickness. Adoption of a 3D analysis approach is essential in obtaining this critical information.

Furthermore, in our study, thresholding was performed manually, resulting in a time-intensive process that is susceptible to human bias.[33] In Figure 2, we visually illustrate the differences between the RGB images of the EF scaffolds (left) and the binary images of the scaffolds. Despite the presence of vessels, their width prevents their detection during the thresholding process, leading to inaccurate quantification values. This observation is evident when comparing scaffolds, which exhibit similar vessel area ratios but clearly show undetected micro-vessels; there is also the fact that thresholding detected the edges of scaffolds and took them into count as if they were vessels. A recent study employed ImageJ for comparing vascular area percentages of different types of scaffolds, and similar issues with micro-vessels were detected in macroscopic representations for fibrin/alginate, FACaP1, and FACaP2.[30]

The accurate evaluation of functional perfusion capacity and vessel architecture is crucial in the validation of scaffolds for regenerative medicine applications. This process necessitates using advanced analytical techniques to obtain precise quantitative data. The current studies which employ CAM assay to evaluate in vivo angiogenic response induced by the tested scaffold use Micro-CT as the imaging technique and Microfil as the contrast agent.[16,17] However, Woloszyk et al. identified a limitation regarding the circulation of Microfil during the perfusion process.[16] Since perfusing the heart of a chicken embryo would damage the CAM and its blood vessels, Microfil perfusion is initiated through a vessel on the CAM surface. Consequently, the blood vessels are not perfused through the exchange of Microfil with blood in a closed circulation system. Furthermore, there are several studies done in mice and rats, reporting heterogeneous perfusion of Microfil, especially in smaller blood vessels.[34] While this does not pose a problem when visualizing vessel architecture, it introduces inaccuracies in quantifying angiogenesis due to the vessels that Microfil fails to reach. In line with Woloszyk et al. 's findings, our results confirm that the contrast agent did not reach all vessels present on the CAM surface; therefore, the complete vascular system promoted by scaffolds could not be detected (Figure 3B).

As an alternative to Microfil, we explored using Optiray 350, an iodine-based contrast agent, to visualize angiogenesis within EF scaffolds implanted in a rat model via Micro-CT. Our objective was to achieve high-resolution imaging of the vascular network within the scaffold, with a particular focus on the infiltration of new, small vessels. However, similar to the limitations observed with Microfil, our imaging results demonstrated that only large blood vessels were visible, with no detection of microvessels or capillaries. This outcome suggests that Optiray 350 has limited penetration into smaller-diameter vessels, reducing its utility in capturing the full extent of the microvascular architecture within scaffolds.

The restricted visualization is likely due to the relatively high molecular weight and low osmolality which decreases the diffusion capacity of Optiray 350, which may impede its permeation into fine microvascular networks.[26] Additionally, the scaffold's material properties itself may act as a diffusion barrier, further hindering access to capillary beds. Compounding these limitations is the short half-life of Optiray 350, which ranges from 113 ± 8.4 and 104 ± 15 min.[35] Potentially reducing its effectiveness in maintaining sufficient circulation for comprehensive imaging of vascular structures. As a result, this imaging method, like Microfil, failed to provide a detailed view of the microvascular system essential for accurate quantification of angiogenesis. These findings underscore the necessity of alternative imaging approaches capable of resolving intricate microvascular networks, which are critical for evaluating scaffold performance and integration in regenerative medicine applications.

To address this limitation, we utilized confocal microscopy as an alternative imaging method to visualize the perfusion of ICG dye. Notably much like with Micro-CT, a 3D analysis approach was employed, therefore, our results remained representative of the in vivo conditions.

ICG has a high affinity for albumin and demonstrates rapid and homogeneous distribution within the bloodstream following intravenous administration.[20] Therefore, we investigated the potential of ICG as a superior contrast agent for evaluating the angiogenic properties of scaffold before implantation. The data presented in this study clearly demonstrated a noteworthy disparity in vascular volume ratio between Microfil and ICG, with ICG displaying significantly higher values (Figure 6D); moreover, H&E staining of our scaffold also indicated that the vessels infiltrated inside, supporting the ICG findings (Figure 2C).

Quantitative analysis showed that confocal microscopy could reliably detect vessels within the range of 1–150 µm, whereas Micro-CT failed to resolve vessels smaller than 27 µm due to its lower resolution and incomplete perfusion. These differences in imaging capabilities make confocal microscopy a more precise approach for evaluating the full spectrum of blood vessel thicknesses, thereby providing a clearer understanding of angiogenesis within the tested scaffolds.

In contrast, both Microfil and Optiray 350 exhibited limitations in visualizing microvessels. The high molecular weight and low diffusion capacity of these agents hindered their penetration into fine microvascular networks, while their use in micro-CT was further impeded by incomplete perfusion. Optiray 350, with its short half-life of 1–2 h and low osmolality, particularly struggled to provide a comprehensive view of capillary networks. However, lower molecular weight contrast agents like ICG offer improved efficacy in mapping capillary structures, as evidenced by the presence of thick vessels and microvessels in the z-stacks obtained from ICG dye visualization under the confocal microscope (Figure 4B,D). This capability to capture vessels situated on different planes underscores the optimal performance of ICG in accurately quantifying angiogenesis.

Additionally, adjusting imaging parameters or exploring dual-modality imaging could further enhance capillary visualization, providing a more comprehensive assessment of scaffold vascularization. Optimizing these factors is essential for obtaining detailed angiographic data on capillary networks, which is fundamental for understanding scaffold integration and supporting tissue regeneration. Supporting our findings, a study conducted by Kraft JC et al. mentioned the visualization of 0.2 mm lymph

vessels using ICG, indicating its potential for capturing microvessels.[36]

To the best of our knowledge, we are the first group to use ICG dye, to evaluate angiogenesis on a highly sensitive ex ovo angiogenesis assay. Moreover, the results strongly support the high potential of the ICG dye as a reliable method for accurately quantifying angiogenesis induced by a potential scaffold before its implantation. The focus of our study was to investigate the sensitivity of ICG in detecting smaller vessels that undergo infiltration within the scaffold during the angiogenesis process. The results obtained from our research demonstrated the successful efficacy of our approach in accomplishing this objective. The observed angiogenic response on the CAM is consistent with our expectations, as scaffolds were expected to demonstrate a high degree of vascularization. This strategy offers critical insights into scaffold performance and degradation dynamics, establishing the CAM assay as a powerful intermediate platform for biomaterial evaluation that aligns with the principles of the 3Rs by reducing reliance on vertebrate models. Nonetheless, findings derived from the CAM model must ultimately be corroborated in more physiologically representative animal systems to ensure translational applicability and support progression toward clinical implementation.

4. Conclusion

In conclusion, this study demonstrates the successful development of fibrin–elastin scaffolds with enhanced angiogenic properties and stability, validated using advanced imaging techniques. Among the imaging methods employed, ICG dye combined with confocal microscopy proved the most effective for capturing the full spectrum of blood vessel sizes, including microvessels infiltrating the scaffold. This approach offers a significant advantage over traditional contrast agents such as Microfil and Optiray 350, which exhibited limitations in visualizing smaller vessels crucial for accurate angiogenesis assessment. ICG dye provides a reliable and precise method for quantifying angiogenesis in a physiologically relevant, 3D environment by enabling high-resolution imaging of vascular networks in the CAM assay. Importantly, this methodology aligns with the principles of the 3Rs in research. The CAM assay, when combined with ICG dye and confocal microscopy, reduces reliance on traditional animal models, offering a cost-effective, reproducible, and ethically responsible platform for evaluating biomaterials. By accurately quantifying angiogenesis in vitro, this method allows for the validation of scaffold designs and vascularization potential prior to proceeding to in vivo studies. Integrating the CAM assay with ICG-based imaging represents a transformative approach in tissue engineering, advancing biomaterial research while adhering to the highest ethical standards.

5. Experimental Section

Fabrication of Scaffold: Initial fibrin-only scaffolds were fabricated as previously described.[20] A fibrin solution was prepared dissolving 2% bovine fibrinogen (Sigma, UK) and 10% bovine thrombin (Sigma, UK) in 1 mL of 1× Phosphate buffered saline (PBS). The solution was crosslinked with 3% glutaraldehyde before lyophilization into a disc-shaped scaffold. Preliminary results showed poor stability in the CAM model; therefore, fibrin-only scaffolds were excluded from subsequent experimental procedures and data analysis.

Alternatively, hybrid elastin–fibrin (EF) scaffolds were developed, combining the bioactivity of fibrin with the structural resilience of elastin. The EF scaffolds were fabricated using a 1:1 ratio of elastin and fibrin as previously described.[21] Briefly, a solution was prepared by dissolving bovine elastin powder (Sigma, UK) in 0.5 M oxalic acid ($C_2H_2O_4$) at room temperature. The fibrinogen solution was prepared by dissolving 2% bovine fibrinogen (Sigma-Aldrich, UK) in PBS and mixing it with 1 molar of $CaCl_2$ prior to adding 10 IU of bovine thrombin.[21] The final concentration of proteins was 2% fibrinogen and 10% elastin that were crosslinked with 30 µL of 25% glutaraldehyde (GA) (Sigma-Aldrich, UK). The plates were incubated at 37 °C. The EF scaffolds were lyophilized for 48 h at −55 °C (Alpha 1–2 LDplus freeze dryer, Martin Christ, Germany) (**Figure 7**). Non-crosslinked glutaraldehyde is toxic; hence, scaffolds were washed with 1% sodium borohydride ($NaBH_4$) as a reducing agent to remove excess glutaraldehyde. Final scaffolds were presented in a disk form of ≈10 mm in diameter and 4 mm thickness. Only elastin–fibrin (EF) scaffolds were used for all subsequent implantation, imaging, and quantitative analyses presented in this study.

Pore properties of scaffolds were measured using Micro-CT as described in the previous study.[21] Only fibrin–elastin (FE) scaffolds were used for all subsequent implantation, imaging, and quantitative analyses presented in this study.

Swelling Ratio: The swelling ratio of all scaffolds was determined by applying the following equation:

$$SR = (Mw - Md) / Mw \quad (1)$$

In this equation, Md represents the dry mass of the scaffold, and Mw represents the wet mass of the scaffold. The dry mass of the scaffold was measured initially using a scale, while the wet mass was determined by immersing the scaffold in 2 mL of distilled water for 10 min at 25 °C.

SEM: Scaffolds were prepared for SEM after washing with deionized water to remove excess salts and sputter-coating with a carbon coater. Later, these samples were mounted on stubs. All images were obtained using a secondary electron detector in a Zeiss Sigma 300VP electron microscope with an average working distance of 10 mm.

Ex Ovo CAM Assay: Fertilized chicken eggs were placed in an egg incubator at 38 °C, with 40–60% humidity. On embryonic day (ED) 3, eggs were cracked according to a previously developed method.[30] Viable embryos, covered with a petri dish lid, were transferred to a 37 °C humidified incubator. On ED 9, up to three scaffolds were added to each embryo using sterile tweezers. Scaffolds were placed halfway between the embryo and the outer edge of the CAM and between two large vessels, followed by an additional 3-day incubation period (Figure 7).

Preparation of Indocyanine Green Dye for CAM: The preparation of Indocyanine green was conducted according to the protocol provided by the supplier (Cambridge Bioscience). In sterile conditions, Cayman Chemical's ICG powder was dissolved in an aqueous solvent. 20 mL of sterile water was added to 50 mg of ICG powder, resulting in a final concentration of 2.5 mg mL^{-1}. A total volume of 0.45 mL of the final solution was injected into the CAM.

Preparation of Microfil for CAM: Microfil (Flow Tech, Inc., Carver, MA, USA) was prepared by freshly mixing 80% silicone rubber injection compound MV-122 (yellow), which was diluted in 10% of MV-Diluent and activated by the addition of 10% MV-Curing Agent right before use to prevent early solidification. A total volume of 2 mL of the final solution was injected into the CAM. Later, CAM was covered with a second petri dish and left at 4 °C overnight to allow for polymerization of the dye prior to fixation.

Perfusion of Dyes in CAM Models: On ED 12, surviving CAMs with implanted scaffolds were removed from the incubator. A 3.0x magnifier of the Stuart Colony Counter was used for precision while injecting the dye. Both dyes were injected by using a 0.5 mL syringe into the central vein of the embryo to reach the heart and be distributed to the circulatory system.

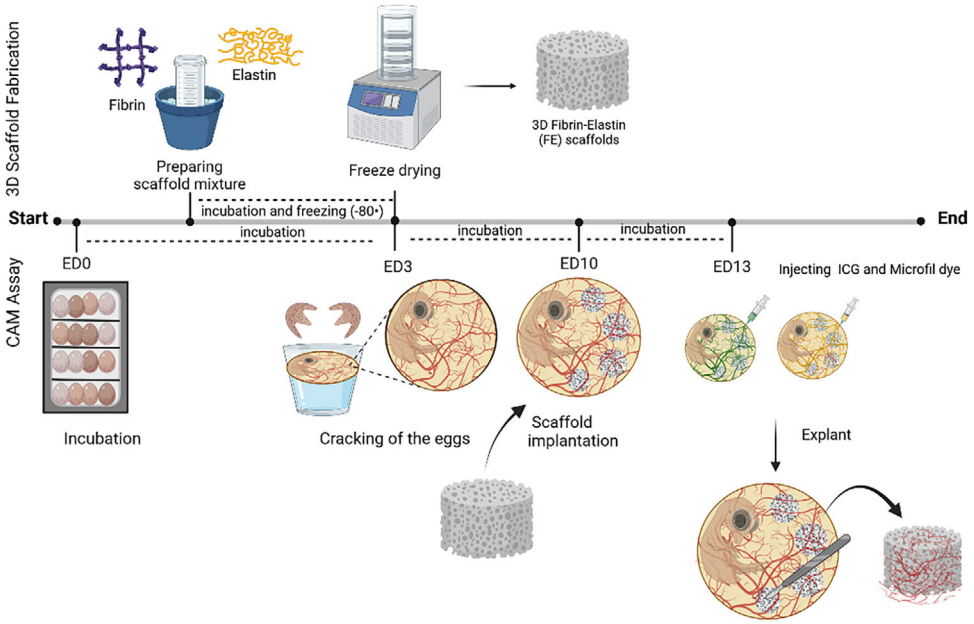

Figure 7. A schematic representation of a methodology used for fabrication of EF scaffolds and CAM workflow.

Medical cyanoacrylate surgical adhesive (Animus Surgical Ltd., U.S.A) was used at the injection site to prevent blood loss and keep embryos alive for ≈20 s.

In Vivo Implantation: The Animal Welfare Ethical Review Body approved (32/018) a rat study. Six Sprague Dawley rats, each weighing ≈350 g, were acclimatized for 14 days before the procedure. The animals were anaesthetized on the day of surgery, and the surgical area was cleaned. A 1 cm midline incision was made in the distal region, two scaffolds were implanted subcutaneously per animal, and the wound site was closed with 3-0 Vicryl sutures. The animals were retained for 14 days. Perfusion of contrast agent in vivo. On day 14, rats were anaesthetized, and 420 mg k^{-1}g Ioversol (Optiray 350 Rx, USA), an iodine-based constant agent, was administered in the left ventricle to visualize angiography of the blood vessel infiltration within the scaffold and five minutes of circulation animals were euthanized. Subsequently, scaffolds were excised and fixed in 10% neutral buffered formalin (NBF) briefly and immediately scanned by Micro-CT for angiography.

Image Analysis: Dissected scaffolds from CAM on ED 13, without the addition of a dye, were captured using a Nikon D3500 digital camera, producing images with dimensions of 6000 × 4000 pixels and 12-bit color depth. These images were analyzed using ImageJ software. Initially, the image underwent a manual cropping process in which the scaffold's surface was delineated to eliminate any background interference and concentrate on the scaffold itself. As this method involved top–down imaging of the exposed scaffold surface, all vessel assessments were inherently restricted to the outermost surface of the scaffold, where the interface with the CAM is most evident. Subsequently, a line was drawn spanning from one end to the other of the scaffold to establish a reference scale. Prior to image processing, the diameter of each scaffold (10 mm) was measured using a ruler, and this known distance was utilized for pixel-to-millimeter conversion. Subsequently, the images were converted into a grayscale format (8-bit), and the threshold was adjusted to measure the fraction of vessels and their respective areas.

Micro-CT: Scaffolds dissected from CAM were kept in 10% NBF (neutral buffered formalin) (Sigma, UK). The samples were removed from NBF and then scanned using X-ray microtomography device Skyscan 1176 (Skyscan 1176, Bruker BioSpin) with the following settings applied to all three samples: 59 kV X-ray voltage, source current 167 µA, 0.6° rotation step, exposure time of 270 ms for each section. The Skyscan NRecon software (Bruker Micro-CT, Belgium) was used to reconstruct 3D models from the scan data. Afterward, the reconstructed dataset was processed to visualize the vessels in 3D space using CTVox software. Parameters such as vessel volume to scaffold porosity, pore thickness, pore range, and vessel thickness were analyzed using CTAn software Version: 1.16.4.1 (Bruker Micro-CT, Belgium).

Confocal Microscopy: Post dissection, scaffolds were examined using a confocal laser scanning microscope (Aurox, UK) to obtain fluorescence images. In this study, a 785 nm laser (for ICG) was utilized along with an 832 nm emission filter (with a bandwidth of 40 nm). The *Z*-axis precision stepper motor was employed to determine depth measurements. For analysis, the acquired *z*-stack was processed using ImageJ software. A macro programming (Figure S1, Supporting Information) was used to convert the area into volume. *Z*-stacks were acquired from the scaffold surface down to a depth of ≈150–200 µm, constrained by fluorescence signal attenuation and tissue scattering. Therefore, the confocal microscopy analysis was limited to the upper layers of the scaffold,

Histology Analysis: Before staining, samples were processed, fixed, and sectioned. To prepare the EF scaffolds for embedding, they were fixed in formalin for 24 h. The scaffolds were cut in half and placed perpendicularly into a paraffin mold to enable cross-sectional visualization. Samples were sectioned at a thickness of 5 µm. Later, the resulting slides were stained with Hematoxylin (Gill's III) and Eosin (0.5% aqueous eosin). Images of the slides were taken with a U-TV0.5XC-3-8 0.5× C-Mount Adapter of an Olympus microscope (Tokyo, Japan) using EPview software. The presence of vessels in each sample was assessed at a magnification of 20×.

Statistical Analysis: Statistical analyses were carried out using GraphPad Prism Version 9.5.1 software. All experiments, except for the 2D quantification of angiogenesis, were performed with a sample size of $n = 3$, representing three independent biological repeats for each condition with appropriate statistical and post-hoc tests. A result was considered statistically significant if the *p*-value was less than 5% ($p < 0.05$), whereas a *p*-value of less than 1% ($p < 0.0001$) was interpreted as statistically very significant.

Supporting Information

Supporting Information is available from the Wiley Online Library or from the author.

Acknowledgements

The authors would like to thank Dr Nicola Mordan from UCL Eastman Dental, Royal Free Hospital, for her assistance with confocal microscopy. This work was supported in part by grants from National Research Foundation, Republic of Korea (RS-2021-NR060095, RS-2024-00348908, RS-2023-00220408).

Conflict of Interest

The authors declare no conflict of interest.

Data Availability Statement

The data that support the findings of this study are available from the corresponding author upon reasonable request.

Keywords

3D biomaterials, angiogenesis, CAM assay, confocal microscopy, micro-CT

Received: February 10, 2025
Revised: June 19, 2025
Published online:

[1] S. Cosson, E. A. Otte, H. Hezaveh, J. J. Cooper-White, *Stem Cells Transl. Med.* **2015**, *4*, 156.
[2] a) A. C. Dudley, A. W. Griffioen, *Angiogenesis* **2023**, *26*, 313; b) A. Fallah, A. Sadeghinia, H. Kahroba, A. Samadi, H. R. Heidari, B. Bradaran, S. Zeinali, O. Molavi, *Biomed. Pharmacother.* **2019**, *110*, 775; c) D. La Mendola, M. L. Trincavelli, C. Martini, *Int. J. Mol. Sci.* **2022**, *23*, 10962.
[3] E. C. Novosel, C. Kleinhans, P. J. Kluger, *Adv. Drug Delivery Rev.* **2011**, *63*, 300.
[4] M. Lovett, K. Lee, A. Edwards, D. L. Kaplan, *Tissue Eng., Part B* **2009**, *15*, 353.
[5] a) J. Yang, S. L. Woo, G. Yang, J. Wang, L. Cui, W. Liu, Y. Cao, *Plast. Reconstr. Surg.* **2010**, *125*, 901; b) C. Ossendorf, C. Kaps, P. C. Kreuz, G. R. Burmester, M. Sittinger, C. Erggelet, *Arthritis Res. Ther.* **2007**, *9*, R41.
[6] H. Shokrani, A. Shokrani, S. M. Sajadi, F. Seidi, A. H. Mashhadzadeh, N. Rabiee, M. R. Saeb, T. Aminabhavi, T. J. Webster, *Int. J. Nanomed.* **2022**, *17*, 1035.
[7] V. Liakouli, P. Cipriani, P. Di Benedetto, P. Ruscitti, F. Carubbi, O. Berardicurti, N. Panzera, R. Giacomelli, *Modern Rheumatol.* **2018**, *28*, 922.
[8] L. Melly, A. Banfi, *Cell Tissue Res.* **2022**, *387*, 451.
[9] V. W. M. van HINSBERGH, A. COLLEN, P. KOOLWIJK, *Ann. N. Y. Acad. Sci.* **2001**, *936*, 426.
[10] a) R. Shaik, J. Xu, Y. Wang, Y. Hong, G. Zhang, *ACS Biomater. Sci. Eng.* **2023**, *9*, 877; b) A. Takei, Y. Tashiro, Y. Nakashima, K. Sueishi, *In Vitro Cell. Dev. Biol.: Anim.* **1995**, *31*, 467.
[11] W. Y. Wang, R. N. Kent, S. A. Huang, E. H. Jarman, E. H. Shikanov, C. D. Davidson, H. L. Hiraki, D. Lin, M. A. Wall, D. L. Matera, J. W. Shin, W. J. Polacheck, A. Shikanov, B. M. Baker, *Acta Biomater.* **2021**, *135*, 260.
[12] C. M. Walthers, A. K. Nazemi, S. L. Patel, B. M. Wu, J. C. Dunn, *Biomaterials* **2014**, *35*, 5129.
[13] Z. Tahergorabi, M. Khazaei, *Iran. J. Basic Med. Sci.* **2012**, *15*, 1110.
[14] C. A. Staton, M. W. Reed, N. J. Brown, *Int. J. Exp. Pathol.* **2009**, *90*, 195.
[15] W. M. S. Russell, R. L. Burch, Methuen & Co. Limited, London, **1959**.
[16] A. Woloszyk, P. Wolint, A. S. Becker, A. Boss, W. Fath, Y. Tian, S. P. Hoerstrup, J. Buschmann, M. Y. Emmert, *Sci. Rep.* **2019**, *9*, 19474.
[17] A. C. Langheinrich, S. Vorman, J. Seidenstücker, M. Kampschulte, R. M. Bohle, J. Wienhard, M. Zygmunt, *Placenta* **2008**, *29*, 937.
[18] H. Kurz, J. Fehr, R. Nitschke, H. Burkhardt, *Histochem. Cell Biol.* **2008**, *130*, 1027.
[19] L. H. Blumgart, *Blumgart's surgery of the liver, biliary tract, and pancreas*, Saunders Elsevier, Philadelphia, PA, USA, **2012**.
[20] P. Sawadkar, N. Mandakhbayar, K. D. Patel, J. O. Buitrago, T. H. Kim, P. Rajasekar, F. Lali, C. Kyriakidis, B. Rahmani, J. Mohanakrishnan, R. Dua, K. Greco, J. H. Lee, H. W. Kim, J. Knowles, E. García-Gareta, *J. Tissue Eng.* **2021**, *12*, 20417314211019238.
[21] P. Sawadkar, N. Mandakhbayar, K. D. Patel, N. Owji, P. Rajasekar, R. Sarama, J. H. Lee, H. W. Kim, J. Knowles, E. García-Gareta, *Macromol. Biosci.* **2024**, *24*, 2400073.
[22] F. J. O'Brien, *Mater. Today* **2011**, *14*, 88.
[23] S. A. Sell, P. S. Wolfe, K. Garg, J. M. McCool, I. A. Rodriguez, G. L. Bowlin, *Polymers* **2010**, *2*, 522.
[24] M. Karsdal, *Biochemistry of Collagens, Laminins and Elastin: Structure, Function and Biomarkers*, Elsevier, London, UK, **2023**.
[25] a) K. Pal, A. T. Paulson, D. Rousseau, Handbook of Biopolymers and Biodegradable Plastics, **2013**; b) A. Jayakrishnan, S. R. Jameela, *Biomaterials* **1996**, *17*, 471; c) N. W. Guldner, I. Jasmund, H. Zimmermann, M. Heinlein, B. Girndt, V. Meier, F. Flüss, D. Rohde, A. Gebert, H. H. Sievers, *Circulation* **2009**, *119*, 1653.
[26] W. H. AlMalki, I. Shahid, A. Y. Mehdi, M. H. Hafeez, *Indian J. Pharmacol.* **2014**, *46*, 251.
[27] A. M. Randi, M. A. Laffan, *J. Thromb. Haemostasis* **2017**, *15*, 13.
[28] L. Zanetta, S. G. Marcus, J. Vasile, M. Dobryansky, H. Cohen, K. Eng, P. Shamamian, P. Mignatti, *Int. J. Cancer* **2000**, *85*, 281.
[29] G. Y. H. Lip, A. Blann, *Cardiovasc. Res.* **1997**, *34*, 255.
[30] N. Kohli, P. Sawadkar, S. Ho, V. Sharma, M. Snow, S. Powell, M. A. Woodruff, L. Hook, E. García-Gareta, *J. Tissue Eng.* **2020**, *11*, 2041731420901621.
[31] E. I. Deryugina, J. P. Quigley, *Methods Enzymol.* **2008**, *444*, 21.
[32] a) A. Guller, I. Kuschnerus, V. Rozova, A. Nadort, Y. Yao, Z. Khabir, A. Garcia-Bennett, L. O. Liang, A. Polikarpova, Y. Qian, E. M. Goldys, A. V. Zvyagin, *Biomedicines* **2021**, *9*, 1578; b) Y. Ma, Z. Zhu, Z. Dong, T. Shen, M. Sun, W. Kong, *Biomed Res. Int.* **2021**, *2021*, 5561125; c) N. Mangir, S. Dikici, F. Claeyssens, S. MacNeil, *ACS Biomater. Sci. Eng.* **2019**, *5*, 3190.
[33] L. Faihs, B. Firouz, P. Slezak, C. Slezak, M. Weißensteiner, T. Ebner, N. Ghaffari Tabrizi-Wizsy, K. Schicho, P. Dungel, *Cancers* **2022**, *14*, 4273.
[34] a) J. C. Schwarz, M. G. van Lier, E. N. Bakker, J. de Vos, J. A. Spaan, E. VanBavel, M. Siebes, *Microsc. Microanal.* **2017**, *23*, 77; b) L. Xie, G. Koukos, K. Barck, O. Foreman, W. P. Lee, R. Brendza, J. Eastham-Anderson, B. S. McKenzie, A. Peterson, R. A. Carano, *Am. J. Physiol., Renal Physiol.* **2019**, *316*, F76; c) X. Liu, T. Terry, S. Pan, Z. Yang, J. T. Willerson, R. A. Dixon, Q. Liu, *J. Vis. Exp.* **2013**, *76*, 50364.
[35] guerbet, SUMMARY OF PRODUCT CHARACTERISTICS **2023**.
[36] J. C. Kraft, P. M. Treuting, R. J. Ho, *J. Drug Targeting* **2018**, *26*, 494.